AD-A192 115 THERMOGRAPHIC DETECTION OF BURIED DEBONDS(U) AEROSPACE 1/1
CORP EL SEGUNDO CA MATERIALS SCIENCES LAB
M T QUINN ET AL. 01 MAR 88 TR-0086A(2935-08)-1
UNCLASSIFIED SD-TR-88-35 F04701-85-C-0086 F/G 17/5.1 NL

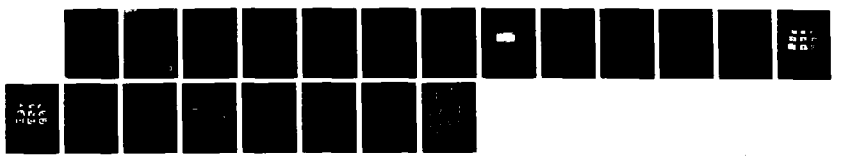

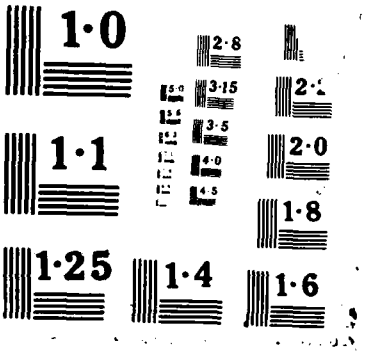
1·0
1·1
1·25
1·4
1·6
1·8
2·0
2·8
3·15
3·5

REPORT SD-TR-88-35

(4)

Thermographic Detection of Buried Debonds

M. T. QUINN, J. R. HRIBAR, R. L. RUIZ, AND G. F. HAWKINS
Materials Sciences Laboratory
Laboratory Operations
The Aerospace Corporation
El Segundo, CA 90245

1 March 1988

Prepared for

SPACE DIVISION
AIR FORCE SYSTEMS COMMAND
Los Angeles Air Force Base
P.O. Box 92960, Worldway Postal Center
Los Angeles, CA 90009-2960

UNCLASSIFIED
SECURITY CLASSIFICATION OF THIS PAGE

REPORT DOCUMENTATION PAGE

1a. REPORT SECURITY CLASSIFICATION Unclassified	1b. RESTRICTIVE MARKINGS
2a. SECURITY CLASSIFICATION AUTHORITY	3. DISTRIBUTION / AVAILABILITY OF REPORT Approved for public release; distribution unlimited
2b. DECLASSIFICATION / DOWNGRADING SCHEDULE	
4. PERFORMING ORGANIZATION REPORT NUMBER(S) TR-0086A(2935-08)-1	5. MONITORING ORGANIZATION REPORT NUMBER(S) SD-TR-88-35
6a. NAME OF PERFORMING ORGANIZATION The Aerospace Corporation Laboratory Operations 6b. OFFICE SYMBOL (If applicable)	7a. NAME OF MONITORING ORGANIZATION Space Division
6c. ADDRESS (City, State, and ZIP Code) El Segundo, CA 90245	7b. ADDRESS (City, State, and ZIP Code) Los Angeles Air Force Base Los Angeles, CA 90009-2960
8a. NAME OF FUNDING / SPONSORING ORGANIZATION 8b. OFFICE SYMBOL (If applicable)	9. PROCUREMENT INSTRUMENT IDENTIFICATION NUMBER F04701-85-C-0086-P00016
8c. ADDRESS (City, State, and ZIP Code)	10. SOURCE OF FUNDING NUMBERS PROGRAM ELEMENT NO / PROJECT NO / TASK NO / WORK UNIT ACCESSION NO

11. TITLE (Include Security Classification)
Thermographic Detection of Buried Debonds

12. PERSONAL AUTHOR(S)
Quinn, Mary T.; Hribar, John E.; Ruiz, Raymond J., and Hawkins, Gary F.

13a. TYPE OF REPORT	13b. TIME COVERED FROM _____ TO _____	14. DATE OF REPORT (Year, Month, Day)	15. PAGE COUNT
		1988 March 1	18

16. SUPPLEMENTARY NOTATION

17. COSATI CODES			18. SUBJECT TERMS (Continue on reverse if necessary and identify by block number)
FIELD	GROUP	SUB-GROUP	

19. ABSTRACT (Continue on reverse if necessary and identify by block number)

A study was done to test the sensitivity of infrared video imaging for detecting adhesive bonding flaws underneath 0.375 in. of steel and 0.25 in. of rubber insulation. Thermographic resolution from heat application was determined experimentally. In addition, a computer model of the specimen's thermal response was investigated using finite element analysis.

20. DISTRIBUTION / AVAILABILITY OF ABSTRACT	21. ABSTRACT SECURITY CLASSIFICATION
☐ UNCLASSIFIED/UNLIMITED ☒ SAME AS RPT ☐ DTIC USERS	Unclassified
22a. NAME OF RESPONSIBLE INDIVIDUAL	22b. TELEPHONE (Include Area Code) / 22c. OFFICE SYMBOL

DD FORM 1473, 84 MAR 83 APR edition may be used until exhausted
All other editions are obsolete

SECURITY CLASSIFICATION OF THIS PAGE

UNCLASSIFIED

CONTENTS

FIGURES

I. INTRODUCTION

This study was done to improve the reliability of solid rocket motors by testing infrared video imaging for detecting adhesive bonding flaws. The flaws, buried beneath 0.3 in. of steel and 0.2 in. of rubber in these motors, have been difficult to detect by conventional pulse-echo ultrasonic techniques. Ultrasonic inspection has been ineffective because of the large acoustical impedance mismatch at the steel-rubber interface. To detect buried flaws in spite of the impedance mismatch, infrared video imaging was investigated.

II. EXPERIMENTAL TESTING

To test the sensitivity of infrared video imaging, three test specimens were fabricated. Each specimen was made of 0.32 in. of 4340 steel bonded to 0.2 in. of silica-filled nitrile butyl rubber (NBR) insulation that was bonded to 3.0 in. of simulated propellant (Fig. 1). To simulate an adhesive bonding flaw, or a debond, a 0.10 in. deep square area was removed from the middle of the propellant before it was bonded to the NBR. Three debond sizes were tested, which were square areas with sides 2.5, 3.0, and 3.5 in. long. The exposed steel was painted with a white vinyl paint to simulate the solid rocket motor. The paint changed the emittance of the steel to 0.95 at the wavelength used by the infrared video imaging system.

An Inframetrics model 600 infrared camera was used for this study. The system comprises a detector and its electronics, a monitor, and a video cassette recorder (VCR). The HgCdTe liquid nitrogen cooled detector has a spectral sensitivity of 8 to 12 μm radiation. Without averaging, the system can detect temperature differences as small as 0.36°F. The monitor was used for real time viewing of the specimen. All data from the detector were recorded on tape with the VCR.

The specimens were positioned vertically, 7 ft from the camera, with the steel facing the camera (Fig. 2). There were no external heat sources that could reflect radiation off the specimen and cause a false reading. A 2 min pretest was taken of each specimen to ensure thermal stability.

Two techniques were used to apply heat to the specimen: the "water wand" technique and the water bed technique. The first technique used a water wand, which was a loop of copper tubing containing a row of holes (Fig. 3). The wand was attached to a garden hose. The test temperature was determined by the temperature of the water leaving the hose. Water was sprayed through the wand onto the surface of the steel for 1 min. Excess water was then blotted from the surface of the steel, and the subsequent cooling pattern was recorded for 10 min. Three different temperatures were tested: 75.0-80.0, 95.0-100.0, and 110.0-150.0°F.

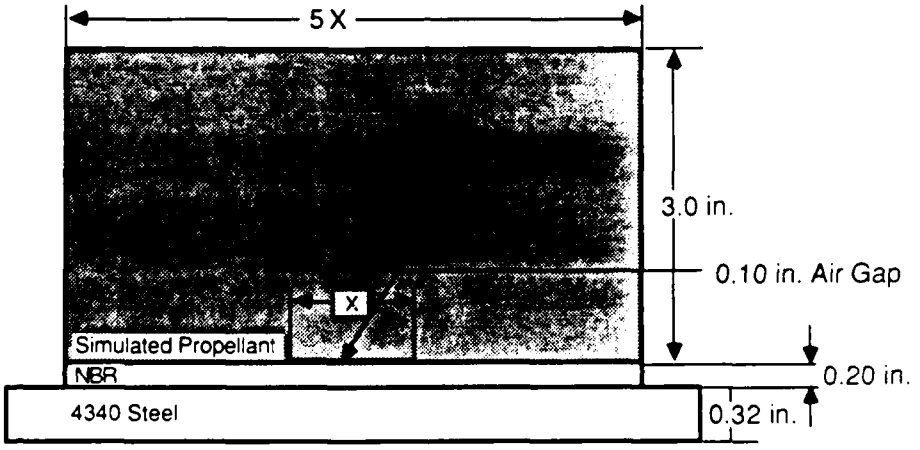

Fig. 1. Schematic of Test Specimen Debond Sizes x = 2.5, 3.0, and 3.5 in.

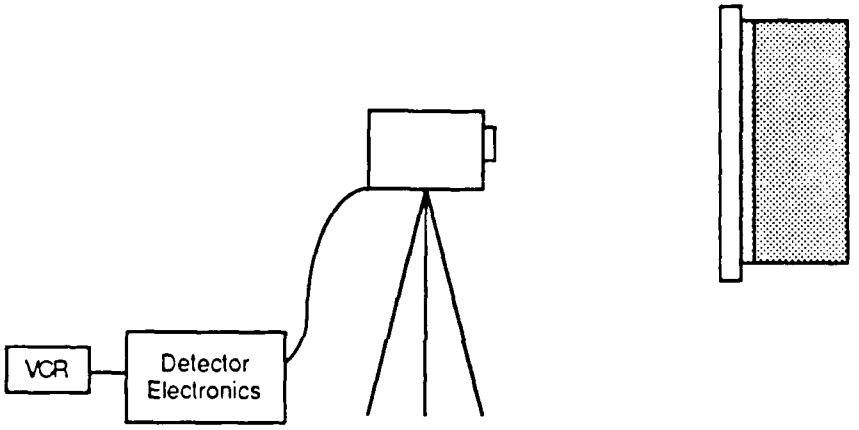

Fig. 2. Test Schematic

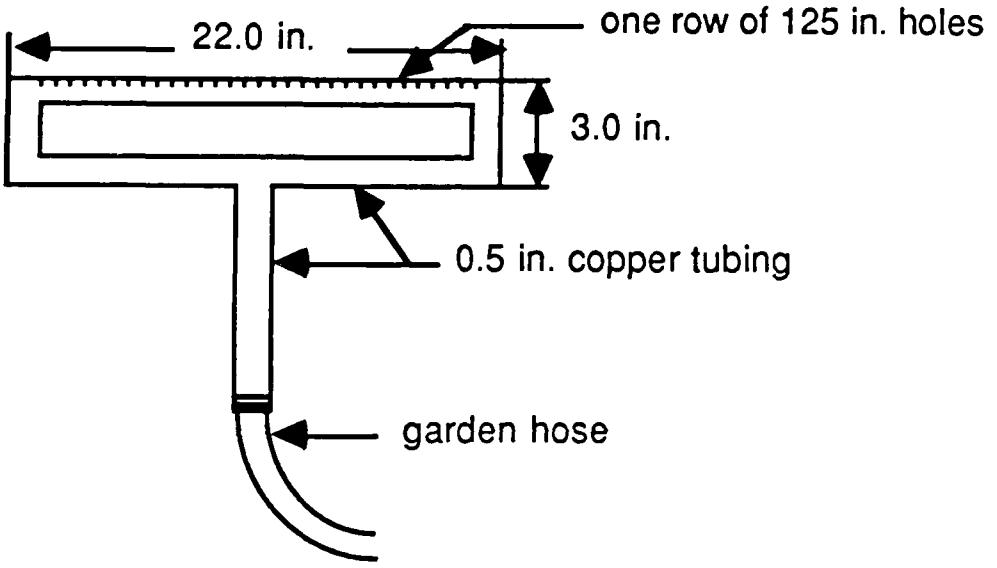

Fig. 3. Schematic of Water Wand

The second technique used a water bed filled with hot water. The test temperature was monitored by a thermocouple placed on the surface of the bed. The specimen was placed steel-side down onto the bed for 1 min. The water bed was agitated during testing to ensure even heating. After heating, the specimen was returned to the vertical position, and the cooling pattern on the steel was recorded for 10 min. Three different temperatures were tested: 110.0-115.0, 124.0-129.0, and 139.0-144.0°F.

Data were obtained at a standard television rate of 60 fields/sec. The system's electronics was set to average 16 fields together, using an exponential averaging algorithm. Averaging the fields reduced the random noise content of the thermal image by a factor of 4. Best results were obtained with the camera's sensitivity range set at 9.0°F. The data on the tape were then fed into an IBM AT computer equipped with the Thermagram thermal image processing system from Thermoteknix Systems, Ltd. The data were averaged again during image processing. Sixteen fields acquired at a rate of 1 field/sec were averaged together to obtain one picture.

III. EXPERIMENTAL RESULTS AND DISCUSSION

Test results using the water wand and water bed techniques are shown in Figs. 4 and 5. Each shade of gray represents an 0.6°F temperature range. During cooling, the surface above a debonded area appears warmer than its surroundings. This occurred because the air gap of the debond restricted the flow of heat through the surface above the debonded area. The temperature difference between the debonded area and its surroundings maximized after a period called the development time. Typically, the debond image develops after 3 to 5 min when the water wand was used and after 5 to 6 min when the water bed was used. The longer development time for the water bed was probably the result of poor heat transfer from the rubber water bed to the specimen.

The success of the water wand or water bed was dependent on the uniformity of the the applied heat. If one area of the specimen received more heat input than its surroundings, it would appear hotter and could be mistaken for a debond. For example, Fig. 5 indicates that the area just to the left of the debonded area D = 3.5 in., T = 130°F was warmer than its surroundings. However, close observation of the specimen's cooling pattern revealed whether the suspected area was a debond or a hot spot. Figure 6 indicates how hot spots start out hotter and cool off more quickly than debonds. With this knowledge, it was determined that the area shown in Fig. 5 was a hot spot caused by uneven heating and was not a debond.

The larger the difference between the specimen's initial temperature and the applied water temperature, the more difficult it was to heat the specimen evenly. Therefore, debonds were more easily detected at the lower test temperatures.

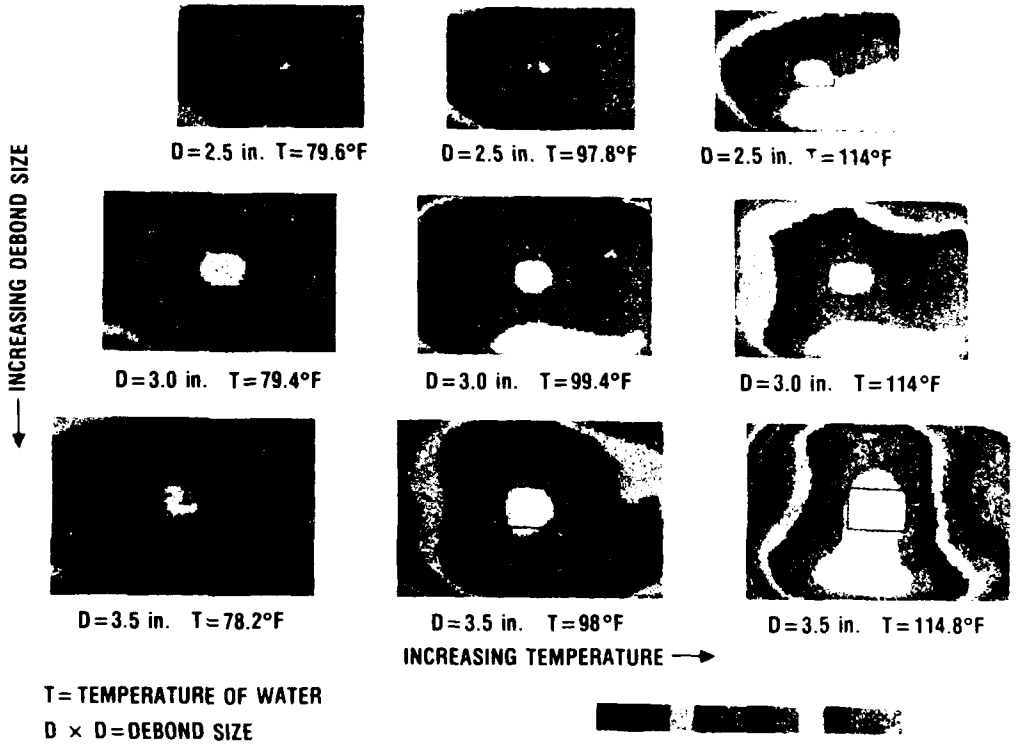

Fig. 4. Results Using Water Wand. Each shade of grey represents 0.1°F. A box is drawn to outline the debond area. Note the increase in temperature gradients with an increase in test temperature.

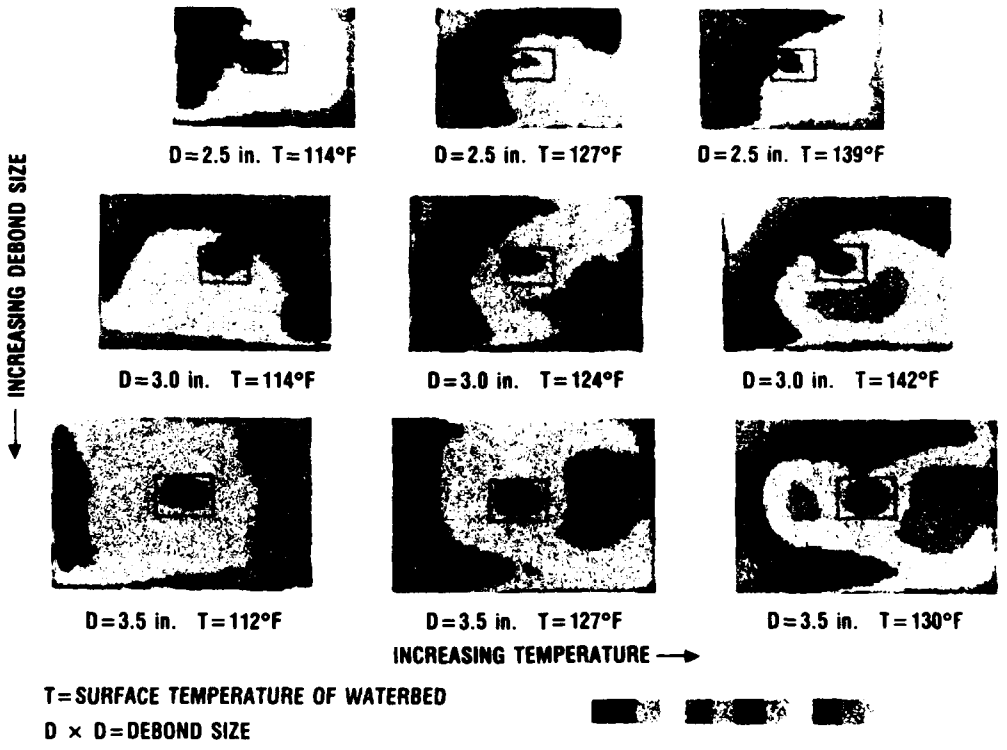

Fig. 5. Results Using Water Bed. Each shade of gray represents 0.6°F. A box is drawn to outline the debond area. Note the nonuniform distribution of heat.

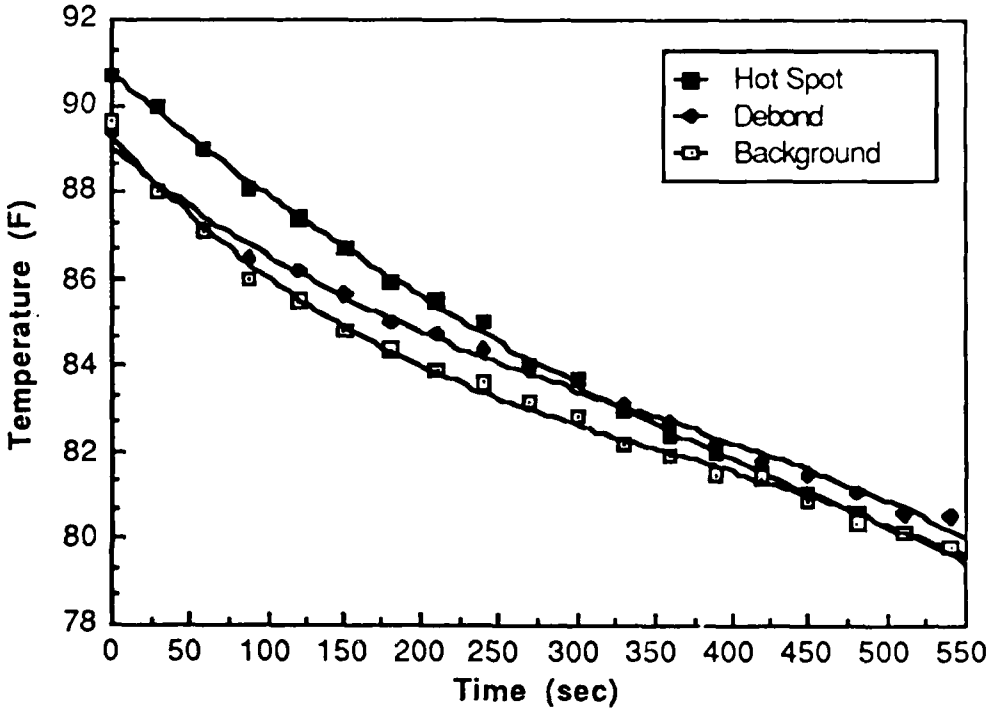

Fig. 6. Cooling Pattern of Three Areas. Note how the hot spot starts out hottest, then dips off to the background temperature. The debond cools off much slower and remains hotter longer.

IV. COMPUTER MODELING

A finite element model of the specimens was prepared using ANSYS® versions 4.2 and 4.3. The model had the same geometric and physical properties as the specimens, except that it had cylindrical symmetry (see Fig. 7). The boundary conditions for the model included a uniform initial ambient temperature. The metal face was forced to remain at 40°F above ambient temperature for 1 min. After heating, the model was permitted to cool by convection. The model of the specimen exhibited cooling patterns similar to those found during the experimental testing.

The model was then used to study the effect of material property changes. Figure 8 illustrates the relationship between the apparent debond radius and time. The apparent debond radius was defined as the distance from the center of the hot spot out to an area 0.6°F lower in temperature. The temperature difference was selected because 0.6°F was the difference required by the thermal imaging system to give a separate color band. In Fig. 8, the first three curves illustrate the effects of increasing the conductivity of the metal surface. The fourth curve illustrates the effect of replacing the metal with insulation.

The results indicate that as the conductivity increases, the development time also increases, and the apparent bedond size decreases. When insulation is used, the development time increases dramatically. This increase was the result of the additional time required for the surface energy to diffuse into the interior of the material, interact with the debond, and return to the surface.

When the material properties were changed to represent aluminum, the radial conductivity effectively shorted out the effects of the debond and did not permit a surface temperature difference of 0.6°F (Fig. 9).

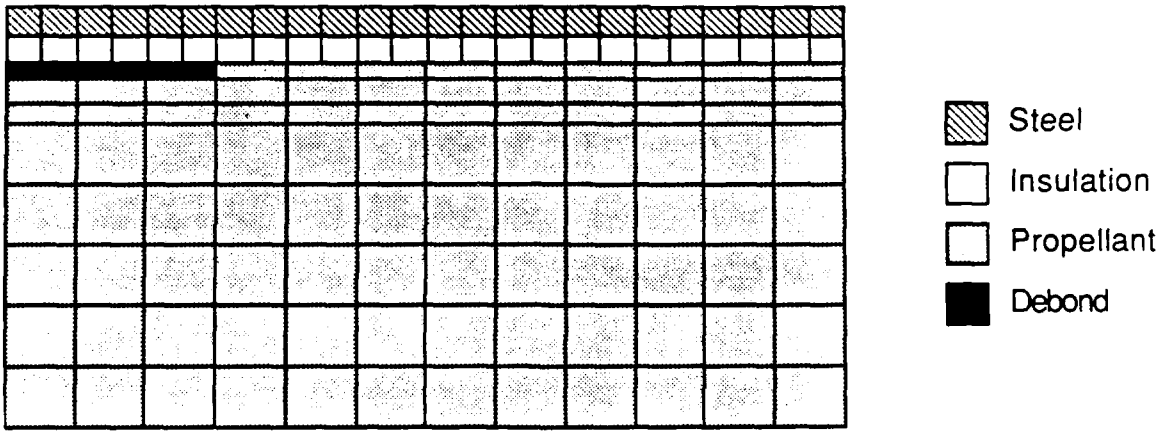

Fig. 7. Finite Element Model. For modeling, the steel layer was modified. Note the model has cylindrical symmetry about the left axis.

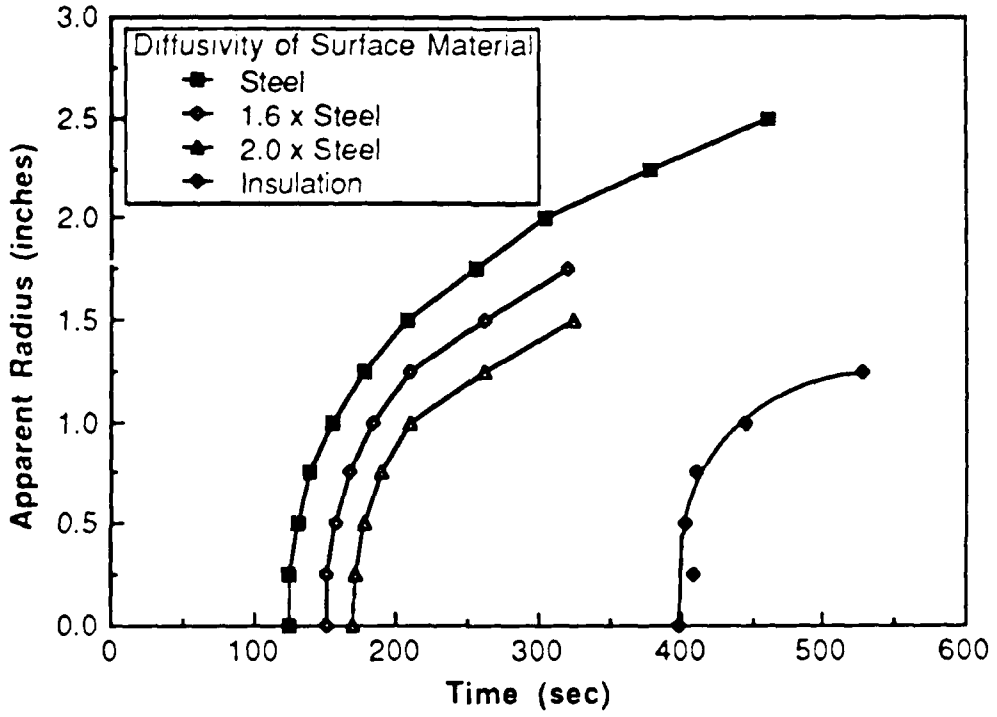

Fig. 8. Apparent Debond Size vs Time. Note that a debond is only visible if it is 0.6°F warmer than the surrounding area.

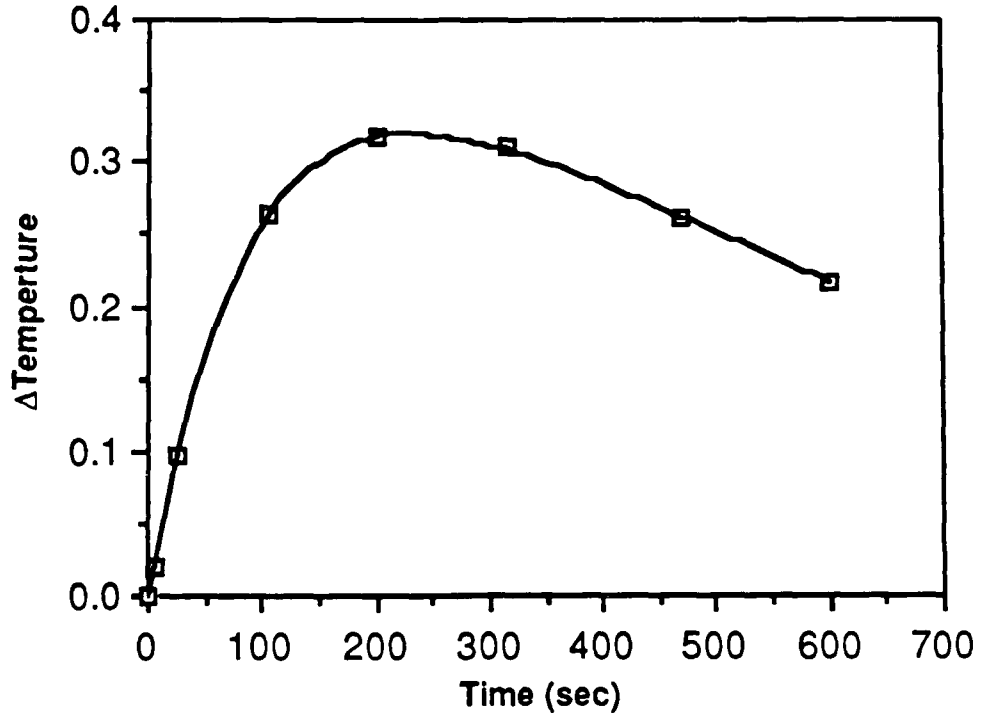

Fig. 9. Temperature Decay of a Debonded Area with Respect to Its Surroundings When Aluminum Is Substituted for Steel.

V. CONCLUSIONS

Thermographic techniques can reliably detect debonds well below the surface of materials. The largest source of error is the result of uneven heating, which can be accounted for by careful analysis of the data. Finite element analysis of the structure adequately modeled the thermal experiments and has shown that debonds can be detected underneath a wide range of materials. (Only materials with a thermal diffusivity near that of aluminum can effecively short out the effect of the debond.)

END

DATE

FILMED

5-88

DTIC